

Contents lists available at ScienceDirect

Materials Characterization

journal homepage: www.elsevier.com/locate/matchar





Dielectric properties of polymer nanocomposite interphases from electrostatic force microscopy using machine learning

Praveen Gupta^a, Linda S. Schadler^b, Ravishankar Sundararaman^{a,*}

- ^a Department of Materials Science and Engineering, Rensselaer Polytechnic Institute, Troy, NY 12180, United States
- ^b College of Engineering and Mathematical Sciences, University of Vermont, Burlington, VT 05405, United States

ARTICLE INFO

Keywords: Electrostatic force microscopy Polymer nanocomposites Finite element analysis Machine learning

ABSTRACT

Interphase regions in polymer nanocomposite materials are difficult to characterize due to their nano-scale dimensions. Electrostatic force microscopy (EFM) provides a pathway to local dielectric property measurements, but extracting local dielectric permittivity in complex interphase geometries from EFM measurements remains a challenge. We demonstrate the efficacy of machine learning (ML) models to extract interphase permittivity using a data set of synthetic EFM force gradient scans generated by finite element simulations. We show that both support vector regression (SVR) and random forest (RF) algorithms are able to 'invert' the force gradient scan to predict the permittivity with high accuracy. Feature reduction by principal component analysis (PCA) improves the model's performance and reveals force gradient contrast to be the most important feature in permittivity detection. We find that these ML models perform better than analytical approaches by capturing significant geometric complexity of EFM measurements.

1. Introduction

Nanoscale fillers dispersed in a polymer matrix can substantially enhance mechanical, thermal and dielectric properties of polymer nanocomposites materials, resulting in their potential widespread use in energy storage and conversion, biomedical, electronics, automotive, packaging and coating applications [1–7]. This enhancement in properties depends critically on the properties and volume of the interphase [8]: a nanosized region surrounding the filler with properties different from both the particle and the matrix. As the size of the filler decreases, the effective interphase region can dominate the properties of polymer nanocomposites. However, the nanometer-scale of the interphase falls below the spatial resolution of many experimental measurement techniques making quantitative characterization of interphase properties a challenge.

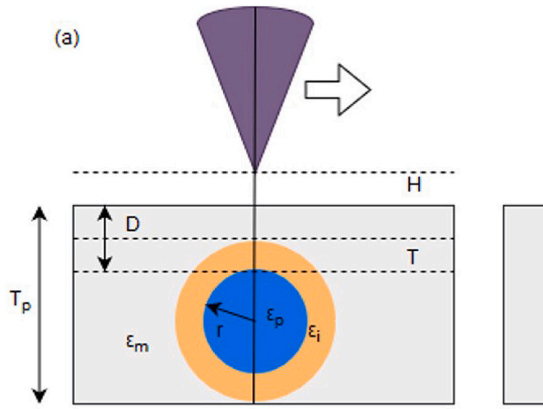
A key potential application of polymer nanocomposites is for highvoltage insulation and capacitive energy storage, which is determined by dielectric permittivity and breakdown strength. Fillers can increase the effective dielectric permittivity without compromising, or in some cases even enhancing, the high breakdown strength of the matrix [9]. However, the effective bulk permittivity does not follow the rule of mixtures and depends on the modified dielectric response from the interphase region. For example, the nanofiller surface can restrict motion of polymer chains reducing the effective permittivity [10]. Consequently, rational design of polymer nanocomposites for dielectric applications requires accurate experimental measurement of the interphase dielectric properties.

Electrostatic Force Microscopy (EFM) is a promising approach for measuring local dielectric properties [11,12]. A member of the Atomic Force Microscopy (AFM) family of techniques, EFM uses a potential applied between a conductive tip and an underlying substrate to measure changes in electric force due to the local dielectric environment. EFM can provide sub-pico newton resolution and high lateral sensitivity [13], but requires careful analysis to extract dielectric properties from the measured forces gradients.

Quantifying local dielectric constants using EFM is difficult primarily because the measured signal depends on the geometric parameters of the tip and on the dielectric variation within an extended region of the sample in a convolved fashion. This necessitates a theoretical model that precisely captures the electrostatic interaction between the tip and the sample with specified geometric and dielectric variation parameters. The complexity of the geometry precludes general analytical solutions, and previous studies have relied on several approximations [14–17]. For example, Fumagalli et al. 2007 [17] presented an analytical model to

E-mail address: sundar@rpi.edu (R. Sundararaman).

^{*} Corresponding author.



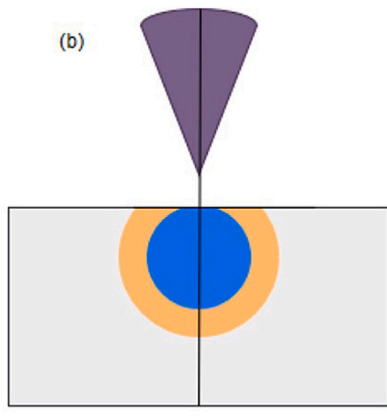


Fig. 1. Schematic of interaction of EFM tip with a nanoparticle-interphase assembly inside a polymer matrix with all the parameters. As the tip scans across the particle, change in local capacitance leads to changing force experienced by the probe which can be used to estimate interphase permittivity. Particle depth (D) and interphase thickness (T) are also unknown in the setup. Variation in particle depth leads to two different configurations: (a) both interphase and particle are buried within the matrix, and (b) the top of the substrate cuts the interphase with the limiting case (D = 0) shown where it touches the top of the particle.

quantify the permittivity of a dielectric thin film with a truncated sphere cone tip model. They further used this analytical approach to measure the effective permittivity of a core-shell like structure [13], which has since been adopted for quantifying the interphase permittivity [18,19].

However, the use of a thin-film analytical model to approximate a core-shell interphase geometry is only valid under special circumstances, such as when the interphase is exposed to the surface and the particle size is much larger than the tip radius. Further, the thickness of the interphase region and depth of the nanoparticle from the material surface strongly impact the EFM signal and are required inputs to such analytical models, but are unknown in the experimental setup. These complications make it difficult to rigorously quantify interphase dielectric properties from analytical EFM modeling.

The key challenge in EFM modeling for extracting interphase dielectric response is the large number of parameters (geometry, dielectric variation) and measurements (2D arrays of force gradients). Machine Learning (ML) algorithms have been highly successful for recognizing patterns and fitting models, especially in large and complex data sets. In particular, techniques such as Support Vector Machines, Decision Trees and Artificial Neural Networks work readily with high dimensional data [20–23], where analytic approaches are limited. Consequently, these approaches could be valuable in extracting maximal information from EFM measurements, but they have not yet been explored for interphase dielectric measurements.

In this article, we demonstrate the potential of ML techniques to extract dielectric permittivity of interphase regions in polymer nanocomposite materials using "synthetic EFM measurements" generated using finite-element simulations of spherical nanoparticles with annular interphase regions in a polymer matrix. We first investigate a twounknown case where particle depth and interphase dielectric constant are unknown, but the interphase thickness is assumed to be known. We show that from a modest database of 200 finite-element simulations, ML models can predict interphase permittivity with a typical accuracy of 0.24 (mean absolute error). We then investigate a case where interphase thickness is also assumed unknown and demonstrate that the models continue to achieve an impressive accuracy of 0.45 for the extracted interphase permittivity. We use principal component analysis to identify the most important features used by the ML models such as the force gradient contrast, and to filter out spurious features and noise to improve the performance of the models.

2. Methods

Fig. 1 schematically illustrates the working principle of EFM for local dielectric measurements. An external AC and DC voltage is applied to a metallic tip mounted on a cantilever, forming a local capacitor, that is then raster-scanned across the sample. The varying capacitance as the tip moves changes the force on the probe, altering the amplitude,

Table 1 Parameter values and ranges used to generate force gradient scan from finite element simulations. ϵ_i and D were varied to generate the dataset for two unknowns case, while ϵ_b T and D were varied in three-unknowns case.

Parameter	Symbol	Two unknown values	Three unknown values
Lift height	Н	8 nm, 12 nm	8 nm, 12 nm
Polymer substrate thickness	T_p	200 nm (fixed)	200 nm(fixed)
Matrix permittivity	ϵ_m	2.5 (fixed)	2.5 nm(fixed)
Nanoparticle radius	r	50 nm (fixed)	50 nm (fixed)
Nanoparticle permittivity	ε_p	10 (fixed)	10 (fixed)
Interphase thickness	Ť	20 nm (fixed)	5-20 nm (variable)
Interphase permittivity	ϵ_i	1-10 (variable)	1-10 nm(variable)
Particle depth	D	0-50 nm (variable)	0-50 nm (variable)

frequency and vibration phase of the oscillating cantilever. The experimentally measured phase of the second harmonic in the cantilever oscillation,

$$\Delta\phi(2\omega) = \frac{Q}{4L}G_{2w} \tag{1}$$

is proportional to the force gradient df/dz, which in turn depends on the local capacitance and permittivity profile [24]. Q is the quality factor of the cantilever oscillator and k is its effective spring constant. In the present work, we focus on finite element simulations of the force gradient, and its inversion to extract the local interphase permittivity.

Table 1 shows all geometric and dielectric parameters required for calculating force gradient in a finite element simulation of the tip sample interaction. We use a truncated cone with a rounded spherical tip to model the probe, and assume spherical nanoparticles surrounded by a concentric interphase shell of unknown permittivity and potentially unknown thickness. The dielectric constant of the polymer matrix and nanoparticle are typically known experimentally, so we hold them fixed across all simulations. However, the extent of the interphase region (interphase thickness) and its dielectric constant depend on the interaction of the matrix with the nanoparticle and the type of nanoparticle surface modification. Additionally, the nanoparticle-interphase assembly can be buried anywhere inside the matrix, and its depth from the surface is not experimentally known a priori. Consequently, the depth, interphase permittivity and interphase thickness are treated as experimental unknowns that are varied to generate the dataset for the ML models.

2.1. Data generation and finite element simulation details

Fig. 2 summarizes our procedure for generating each point in the dataset. We use COMSOL Multiphysics to perform finite element

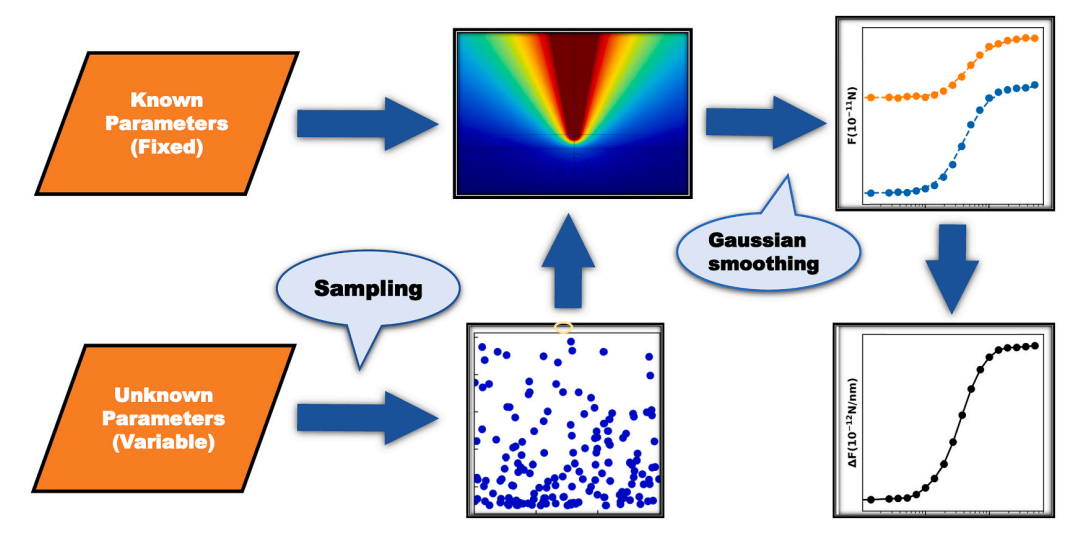


Fig. 2. Procedure for generating the force gradient dataset for the machine learning model. We sampled unknown parameters in a range and generated force curves at two different lift heights. Force gradient scans were produced by numerical differentiation of these force scans. This force gradient dataset was used by ML model to predict unknown parameters.

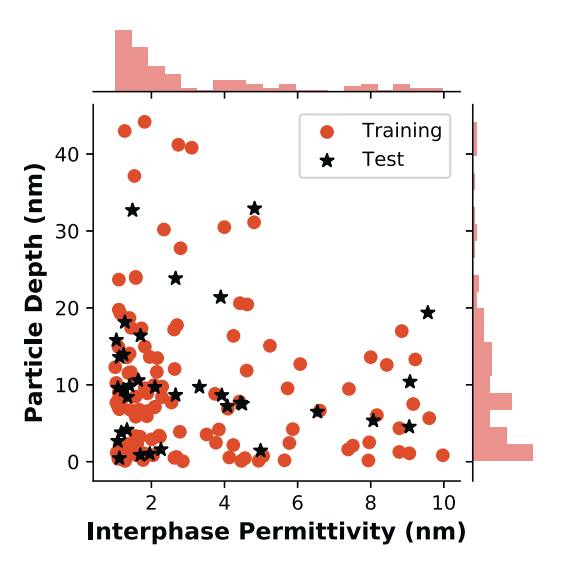


Fig. 3. Sampled distribution of two unknown parameters ϵ_i and D to get higher density of points with low ϵ_i and D (particle closer to the surface).

simulations and generate a force scan for several sets of parameters within the ranges shown in Table 1. Specifically, we use the AC/DC (Electrostatics) module to solve Poisson's equation for the electrostatic potential in the tip-sample system and integrate the Maxwell stress tensor around the tip to calculate the electrostatic force [25]. As the system is axially symmetric along the z-axis, our force scan is parametrized by a single variable x, the horizontal distance of the tip from the top of the particle. We use 21 x-points spaced logarithmically from 1 to 1000 nm in order to better sample the interphase and transition region (rather than the polymer matrix far from the particle). We generate these force scans at lifts height of 8 and 12 nm, applied Gaussian smoothing to reduce noise from meshing changes, and use a finite difference derivative to calculate the force gradient (df/dz) at a lift height of 10 nm. The resulting array of force gradients (at 21 x values) serve as the features for ML modeling, while the 'unknown' variables that are varied in the dataset serve as the targets.

2.2. Unknown parameter sampling

We sample the unknown parameters (targets for subsequent ML modeling): interphase permittivity, particle depth and interphase thickness, in the ranges specified in Table 1. We uniformly sample $1/\epsilon$ in [0.1, 1] to get interphase permittivity values in the range of 1 to 10. We sample particle depth in an exponential distribution with scale parameter 15 nm with an upper cutoff of 50 nm. The bias in sampling interphase permittivity and depth focuses more data points in the training and test sets in the regions where where these parameters that are most likely to be encountered in experiment. Extrinsic interphases typically exhibit lower dielectric constant than the matrix, and the experimental sensitivity decreases dramatically when the particle is buried deeper within the matrix. Consequently, the higher density of points in the dataset for lower permittivity and particle depths (Fig. 3) facilitates more accurate predictions in the experimentally detectable space with a limited dataset size.

A total of 200 such parameter combinations form the data set (test+training) for the first analysis below using two unknowns: the particle depth and interphase permittivity. The interphase thickness is held fixed at 20 nm. In the second analysis below, we additionally let the interphase thickness vary uniformly between 5 and 20 nm for a total of three unknowns and 190 sampled parameter combinations (Fig. 4).

3. Machine learning models and validation

We use Support Vector Regression (SVR) and Random Forests (RF) as implemented in the Python scikit-learn library [28] to build inverse models that extract interphase properties from the force gradient scans. SVR is a kernel-based supervised-learning approach that maps the original data into a high dimensional space and then fits a hyper plane close to as many points as possible [26]. RF is a supervised learning technique based on ensembles of decision trees [27], each of which makes predictions based on decision rules. Both methods exhibit many unique advantages for solving the nonlinear and high-dimensional problems inherent in this study. We use Principal Component Analysis (PCA) to select the most important features as a data preprocessor to these models that reduces redundancy and noise in the input features.

We use 6-fold shuffle-split cross validation to evaluate the performance of different regressors. Specifically, we randomly split the data set into an 84% training and 16% test set six times, and evaluate the average correlation score (CV) and mean absolute error (MAE) for each

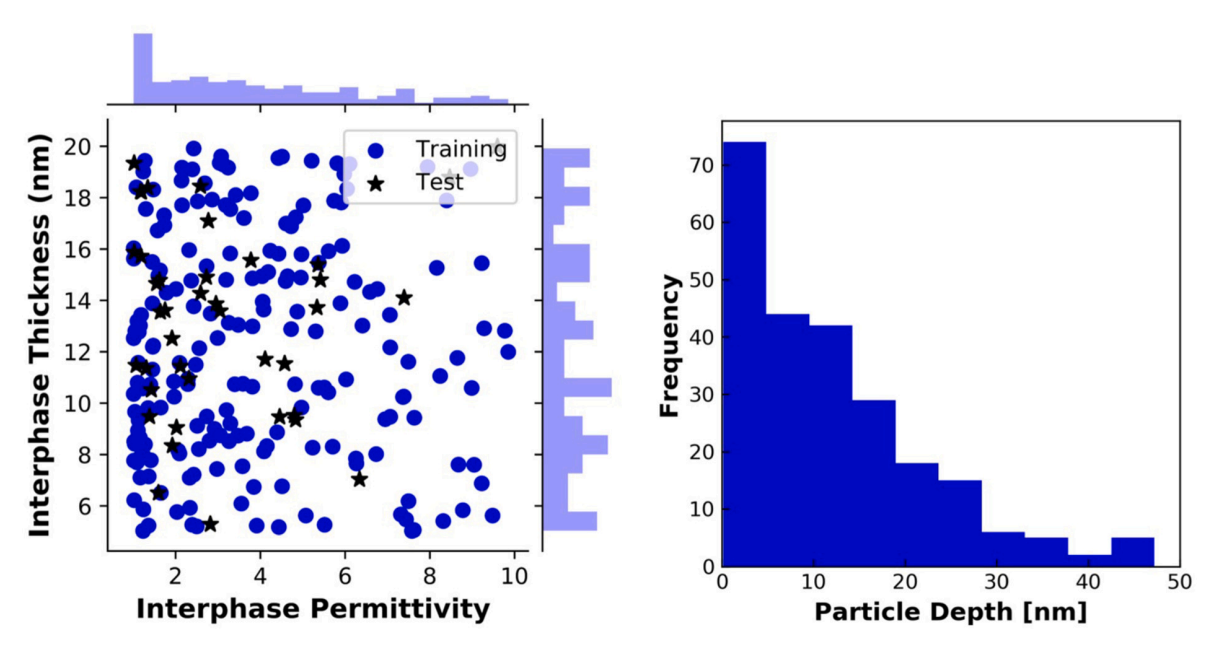


Fig. 4. Sampled distribution of (a) ϵ_i and T, and (b) particle depth, for three-unknown parameter case.

Table 2Performance of regressors for interphase permittivity and particle depth predictions for the two-unknown parameters case. RF(IP) represents random forest regressor with original features for interphase permittivity detection and PCA + SVR(D) represents support vector regressor with 3-PCA components for particle depth detection. Other notations follow the same format.

=				
Model	CV score (%)	MAE (train)	MAE (shuffled)	MAE (test)
RF(IP)	94.7	0.13	6.25	0.25
SVR(IP)	94.5	0.15	8.21	0.24
PCA + RF(IP)	94.0	0.11	3.90	0.27
PCA + SVR(IP)	93.4	0.24	8.25	0.26
PCA + RF(D)	54.6	1.61 nm	32.4 nm	3.55 nm
SVR(D)	59.5	3.06 nm	32.6 nm	3.30 nm

target. We further test for over-fitting by target shuffling i.e. randomly permuting only the target array, which wipes out all correlations. Evaluating a model built on the shuffled data with the same hyperparameters as the original model provides a point of comparison for the MAE. Finally, we test our model's performance on an independent test set of 30 data points for the two-unknowns case and 34 data points for the three-unknowns case. Additionally, the RF regressor provides feature-importance attributes to quantify the relative importance of each feature for the prediction of each target value. We optimize all model hyperparameters systematically using a grid search.

4. Results and discussion

4.1. Two unknown parameters

Table 2 and Fig. 5 show the accuracy of RF and SVR for predicting interphase permittivity and particle depth, when only these two experimental parameters are treated as unknown. Both models perform well for permittivity predictions with high CV ~ 0.94 and low MAE (test) ~ 0.25 , and somewhat less so for particle depth predictions with CV ~ 0.55 and MAE (test) ~ 3.6 nm. Note that MAE of the target shuffled models is consistently around 10 times higher than that of the actual model for permittivity, indicating that it is not overfit. Similarly, the MAEs on the separate test set are slightly higher compared to the training set, but still significantly smaller than the shuffled models, confirming that the model is not over-fit.

We use principal component analysis (PCA) to remove redundant features and noise from the data. The first three principal components (Fig. 6a) capture more than 95% of the variance in the feature data and using them alone improves performance of the regressors. The first component represents the general shape of the force gradient difference from the bulk, varying monotonically from atop the particle (x=0) to zero far away. It predominantly measures the force gradient contrast: the difference between the force gradient value atop the particle and the pure polymer matrix. Fig. 6b indeed shows that the first PCA component correlates linearly with the calculated force gradient contrast for each data point. This feature alone captures 90% of the variance in the data and is the most important feature for permittivity prediction, as also shown by the feature importance attribute chart of random forest regressor in Fig. 10a.

While the first feature captures the force gradient at the top of the particle, the second and third principal components capture the change in force gradient when the tip approaches the interphase-matrix transition region. These components have complicated linear dependence on the scan points around this transition zone and are difficult to identify intuitively. The second PCA feature is more important than the force contrast gradient for particle depth prediction as shown by the feature importance plot (Fig. 10b). Thus, proper identification of particle depth not only requires force gradient contrast between matrix and particle but also how and where the force gradient curve changes as it transitions from interphase to matrix. Overall, this complexity of the particle depth effect on the force gradient scan lowers the accuracy of its prediction.

Force gradient contrast, which we find above to be the most important feature for permittivity prediction of a nanosized object buried in a matrix, has been used previously in analytical approaches. For example, [19] fits an analytical equation for the force gradient based on an approximate model for probe-sample capacitance,

$$C = 2\pi\epsilon_0 R \ln\left(1 + \frac{R(1 - \sin\theta)}{z + h/\epsilon_r}\right),\tag{2}$$

to extract the permittivity of an exposed object (particle or interphase) at a known depth that can be determined from the height scan of the force microscope.

Fig. 7 shows that the interphase permittivity indeed correlates strongly with the force gradient contrast (first PCA feature), but there is

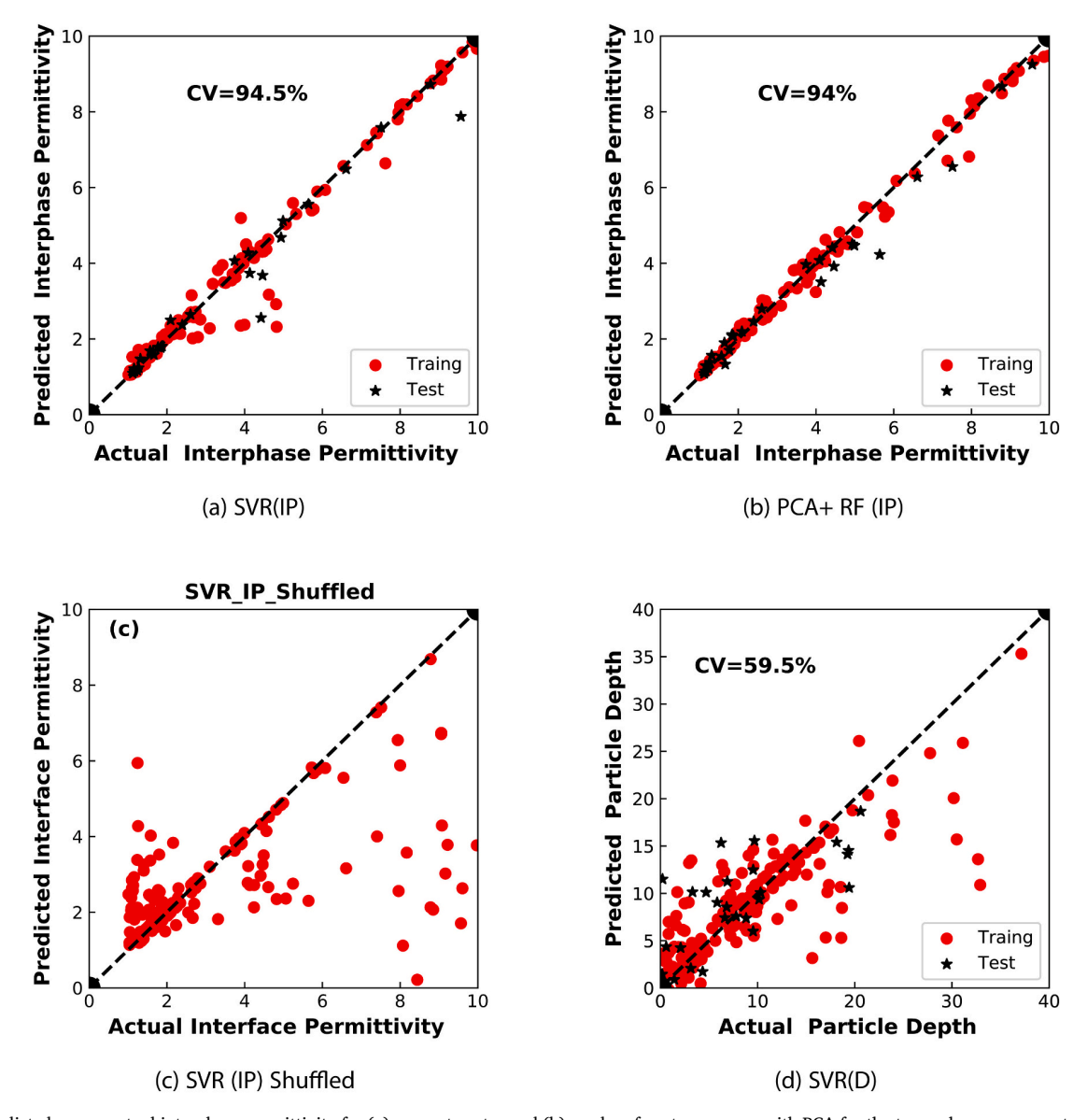


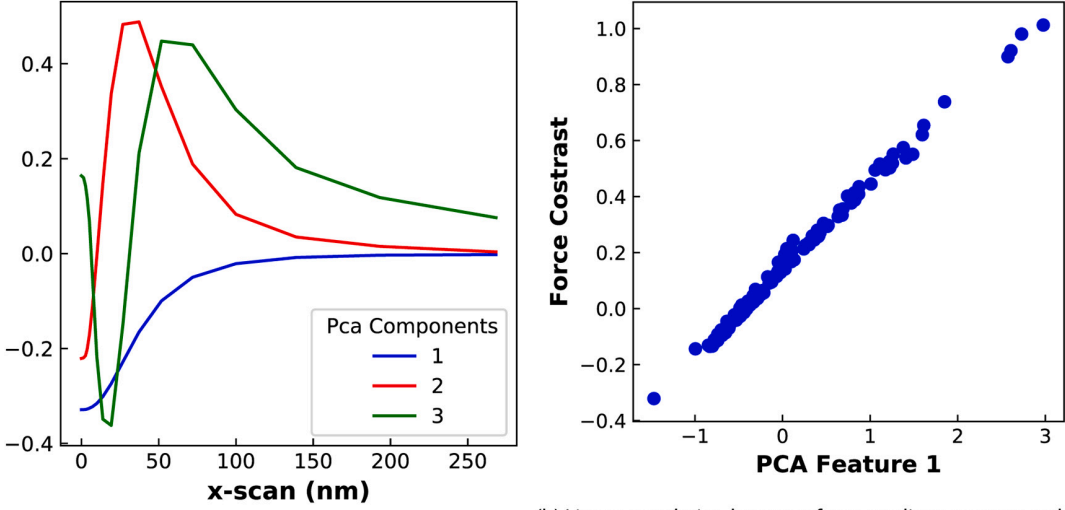
Fig. 5. Predicted versus actual interphase permittivity for (a) support vector and (b) random forest regressors with PCA for the two unknown parameters case. Both regressors predict permittivity with high accuracy in the given range. (c) Target shuffled plot for Random forest with PCA has the baseline prediction with much higher MAE compared to the original model. (d) Models or extracting depth information from the force gradient scans exhibit lower CV compared to those for permittivity extraction.

a large spread corresponding to variation in particle depth. Consequently, when we apply the analytical approach to the more general situation of buried nanoparticles, we find a much larger MAE of 1.42 in the extracted permittivity. Using numerical simulations of the force gradient contrast (first PCA feature) brings the MAE down to 0.64, while the addition of second and third PCA components further reduces the MAE to 0.27 in the permittivity. (See Table 3.) This indicates that even though the force gradient is the most important feature, changes in the shape of the curve around the interface-matrix assembly are also important and cannot be neglected for accurate permittivity prediction. Additionally, Fig. 8. shows that using the three most important PCA features reduces outliers compared to directly using the full force curves.

4.2. Three unknown parameters

Table 4 compares the accuracy of the models when the interphase thickness is assumed to also be unknown, for a total of three unknowns. As expected, addition of a third unknown parameter lowers the performance for all the models. For this more complex dataset, SVR with all features works the best with an impressive MAE of \sim 0.45. For RF regressors, we observe large outliers in permittivity predictions with the original features (Fig. 9). Fortunately, using PCA with three components dramatically improves the performance of the model and eliminates these outliers. Reduced features, with a high variance each, make decision trees splitting at each node more efficient, thereby improving the model's performance.

Force gradient contrast is still the most important feature for the prediction, as shown in Fig.~10a, but its relative importance decreases



(a) Feature representation in the PCA space

(b) Linear correlation between force gradient contrast and PCA feature 1.

Fig. 6. a) Principal components of the force gradient features: the first principal component captures the overall contrast in force gradient contrast as shown by (b) correlation between PCA feature 1 and the force gradient contrast. Second and third components capture changes around the interphase/particle-matrix region centered around 50 nm (diameter of the nanoparticle). Combined, these three features capture more than 95% of the variance in data and are most important for permittivity extraction.

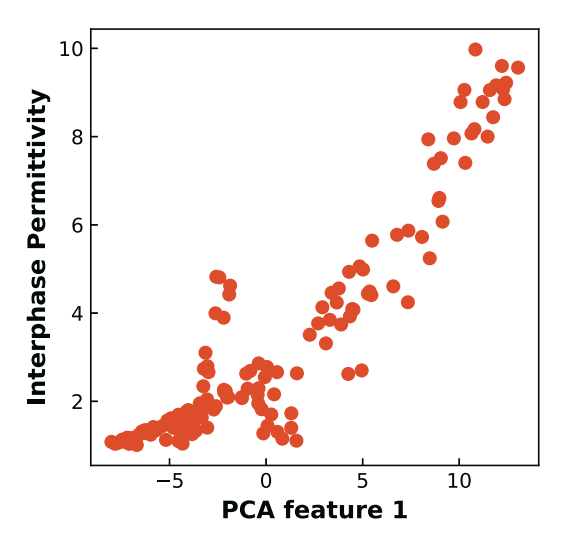


Fig. 7. Variation of interphase permittivity with the first PCA feature (force gradient contrast) for the two unknown parameters case. The observed spread in the data is predominantly due to variation in particle depth at the same permittivity value, and necessitates the inclusion of additional PCA features for accurate predictions.

Table 3
Performance of analytical model and RF regressors with varying numbers of PCA features: the ML model with a single PCA feature improves substantially on the analytical model, and additional PCA features further reduce MAE in the predictions.

Model	Error in prediction (MAE)
Analytical	1.42
PCA-1 + RF(IP)	0.64
PCA-2 + RF(IP)	0.34
PCA-3 + RF(IP)	0.27

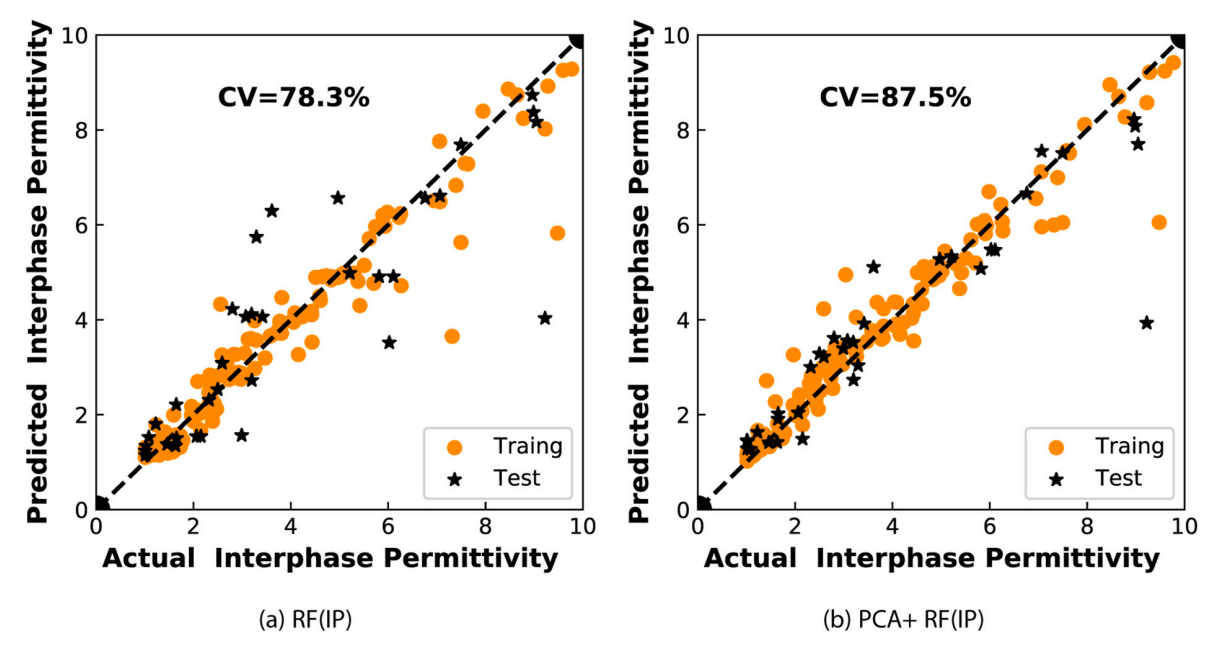


Fig. 8. Predicted versus actual interphase permittivity for Random forest regressor (a) without PCA and (b) with PCA. The outliers in (a) are eliminated by using 3 principal components leading to a higher CV score and lower MAE.

 $\label{thm:problem} \textbf{Table 4} \\ \textbf{Performance of various models for interphase permittivity, particle depth and interphase width predictions for the three-unknown parameters case. Most regressors predict interphase permittivity with high correlation score. Predictions for particle depth - PCA + RF(D), PCA + SVR(D) and interphase thickness - PCA + RF(T) have low CV score because of their complicated co-dependence. \\ \\$

Model	CV score(%)	MAE (train)	MAE (shuffled))	MAE (test)
RF(IP)	78.3	0.60	8.61	0.68
SVR(IP)	88.4	0.43	9.40	0.45
PCA + RF(IP)	87.5	0.46	4.17	0.50
PCA + SVR(IP)	85.2	0.45	9.39	0.67
PCA + SVR(D)	43.3	4.41 nm	31.70 nm	5.30 nm
PCA + RF(D)	33.6	2.21 nm	25.82 nm	4.56 nm
PCA + RF(T)	12.9	3.71 nm	14.21 nm	4.81 nm

relative to the two-unknown parameters case. This is because of a wider spread and more outliers in the functional dependence of the force gradient contrast with interphase permittivity. We identify these outliers as points with low interphase thickness buried deep inside the matrix, for which the permittivity of the matrix, rather than the interphase, dominates the local capacitance (Fig. 9). Thus, the force gradient contrast is very small for these outliers. These outliers expectedly hamper the performance of 1-component PCA with Random Forest, resulting in permittivity errors as large as 6. Addition of the second and third principal components improves the performance drastically on these outliers with the largest error in permittivity prediction of 1.6. Thus, if the interphase thickness is also unknown, using only the force gradient contrast can lead to higher errors in interphase permittivity prediction, necessitating the use of additional features.

The accuracy of these models for particle depth prediction decreases further with three unknowns, primarily because the new unknown, interphase thickness, produces a similar effect on the force gradient as the particle depth. Fig. 10b shows that the second and third PCA features are more important for the prediction of both the interphase thickness and particle depth. This complicated and correlated dependence of these parameters makes it harder for the machine learning model to make accurate predictions for both. Fortunately, these ML models are still able to extract interphase permittivity reliably, despite being unable to

determine the depth and interphase thickness, which would be impossible to do with analytical modeling alone.

5. Conclusion

We show that machine learning approaches can be valuable in extracting interphase permittivity from simulated EFM force gradient measurements of polymer nanocomposite materials. Feature reduction by principal component analysis improved prediction accuracy and showed that force gradient contrast is the most important feature in permittivity detection. However, using only the force gradient contrast can lead to large errors, especially when interphase thickness and particle depth are unknown and other features becomes important. Overall, these models capture significant complexity in the EFM measurements of this system beyond what is possible with previous analytical approaches. In particular, they make it possible to account for unknown experimental parameters such as interphase thickness and particle depth from the force gradient data alone.

Having established the promise of ML modeling for analyzing EFM measurements using synthetic data from finite element simulations, ongoing work in our group applies this methodology to experimental force scans to quantify interphase permittivity in new nanocomposite materials. Additionally, while we focussed here on specialized small data sets with a few (two or three) unknown parameters, future work could build and utilize a large dataset that reliably samples a high-dimensional space of several unknowns. This could facilitate general-purpose EFM analysis of polymer nanocomposites with varying particle sizes and permittivities of both the particle and the polymer matrix.

Data availability

All data and analysis code for the results presented above are included in the supplementary information, along with additional details of the COMSOL simulations used for generating the data.

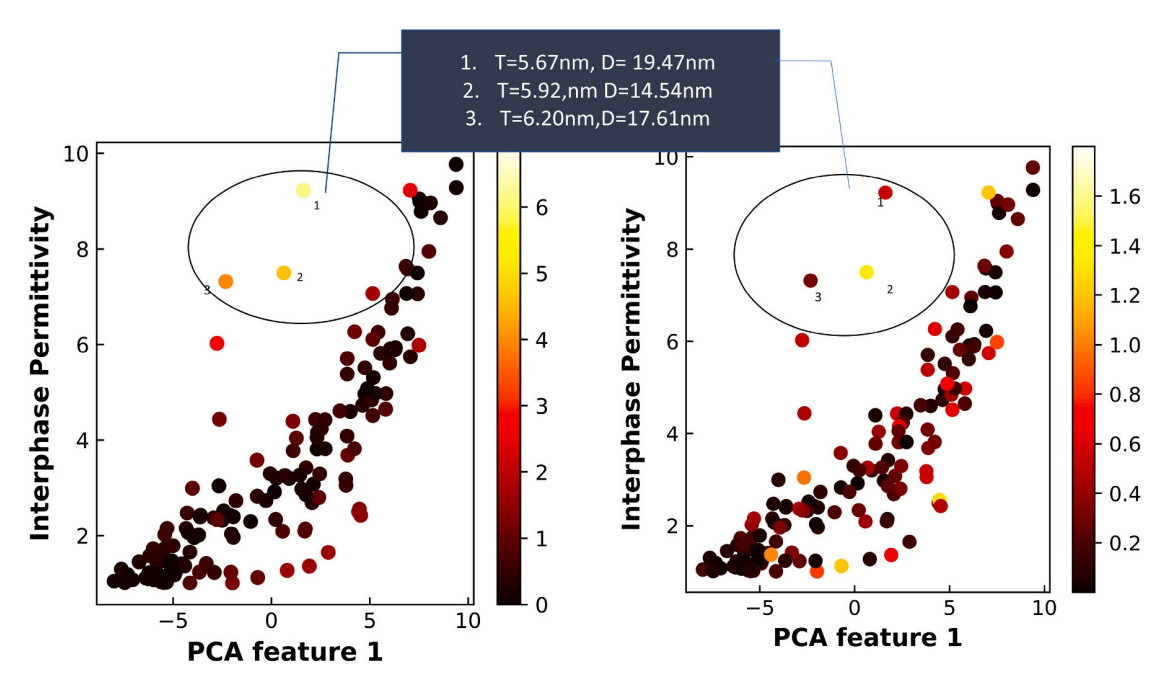
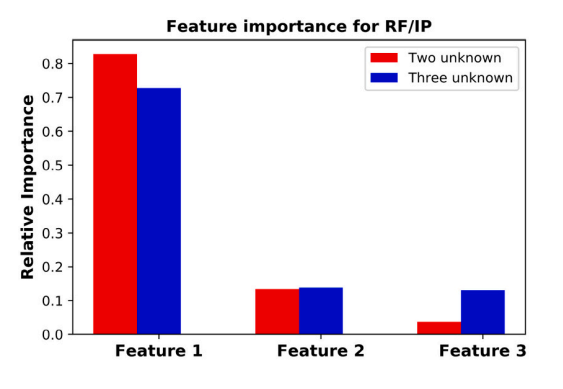
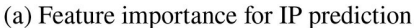
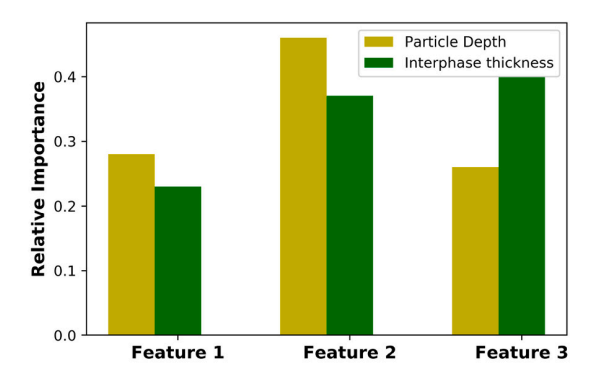


Fig. 9. Interphase permittivity versus PCA feature 1 (force gradient contrast) color mapped with error in permittivity prediction for PCA + RF with 1 feature (left), PCA + RF with 3 features (right) for three unknowns training data. The wider spread and far outliers result in high errors when using a single feature. These outliers correspond to low interphase thickness and particles buried inside the matrix, where EFM is insensitive to the interphase permittivity. Error in prediction for these outliers improves drastically using 3 PCA components.







(b) Feature importance for D and T prediction

Fig. 10. Feature importance of the three PCA components for unknown target predictions using random forest regressor. Force gradient contrast (feature 1) is the most important feature for interphase permittivity detection while features 2 and 3 are more important for particle depth and interphase detection.

Declaration of Competing Interest

The authors declare that they have no known competing financial interests or personal relationships that could have appeared to influence the work reported in this paper.

Acknowledgements

This material is based on the work supported by the National Science Foundation under Grant No. 1729452. All calculations were carried out at the Center for Computational Innovations at Rensselaer Polytechnic Institute.

Appendix A. Supplementary data

Supplementary data to this article can be found online at https://doi.org/10.1016/j.matchar.2021.110909.

References

- [1] L. Ji, P. Meduri, V. Agubra, X. Xiao, M. Alcoutlabi, Graphene-based Nanocomposites for energy storage, Adv. Energy Mater. 6 (16) (2016) 1502159–1515022.
- [2] T. Liu, et al., A graphene quantum dot decorated SrRuO3 mesoporous film as an efficient counter electrode for high-performance dye-sensitized solar cells, J. Mater. Chem. A. 5 (24) (2012) 17848, 17855.
- J. Mater. Chem. A 5 (34) (2017) 17848–17855.
 D.K. Yi, S.T. Selvan, S.S. Lee, G.C. Papaefthymiou, D. Kundaliya, J.Y. Ying, Silicacoated Nanocomposites of magnetic nanoparticles and quantum dots, J. Am. Chem. Soc. 127 (14) (2005) 4990–4991.
- [4] K. Sun, et al., Flexible polydimethylsiloxane / multi-walled carbon nanotubes membranous metacomposites with negative permittivity, Polymer (Guildf) 125 (2017) 50-57
- [5] A.K. Naskar, J.K. Keum, R.G. Boeman, Structural components, Nat. Publ. Gr. 11 (12) (2016) 1026–1030.
- [6] Z. Honarvar, et al., Electronic Physician (ISSN: 2008–5842), Electron. Physician 8 (6) (2016) 2531–2538.
- [7] Z.G. Huige Wei, Yiran Wang, Nancy Z. Shen, Dawaei Jiang, Xingru Yan, Jiahua Zhu, Qiang Wang, Shao Lu, Hongfei Lin, Suying Wei, Smart anticorrosion coatings, J. Mater. Chem. A 3 (2) (2015) 469–480.

- [8] L.S.S.R.C. Smith, J.K. Nelson, Electrical Behavior of Particle-Filled Polymer Nanocomposites 3, 2010, pp. 70–107.
- [9] C.W.N. Yu Song, Shen Yang, Haiyang Liu, Yuanhua Lin, Ming Li, Composites: effects of the shape of the BaTiO 3 nanoinclusions, surface modification and polymer matrix, J. Mater. Chem. 22 (32) (2012) 16491–16498.
- [10] R. Kochetov, T. Andritsch, P.H.F. Morshuis, J.J. Smit, Anomalous behaviour of the dielectric spectroscopy response of Nanocomposites, IEEE Trans. Dielectr. Electr. Insul. 19 (1) (2012) 107–117.
- [11] B. Ju, Y. Ju, M. Saka, Quantitative measurement of submicrometre electrical conductivity, J. Phys. D Appl. Physics 40 (23) (2007) 7467–7470.
- [12] D.C. Coffey, D.S. Ginger, Time-resolved electrostatic force microscopy of polymer solar cells, Nat. Mater. 5 (September) (2006) 21–23.
- [13] L. Fumagalli, D. Esteban-Ferrer, A. Cuervo, J.L. Carrascosa, G. Gomila, Label-free identification of single dielectric nanoparticles and viruses with ultraweak polarization forces, Nat. Mater. 11 (9) (2012) 808–816.
- [14] J. Hu, X.D. Xiao, M. Salmeron, Scanning polarization force microscopy: A technique for imaging liquids and weakly adsorbed layers, Appl. Phys. Lett. 67 (June 1998) (1995) 476.
- [15] Y. Shen, D.M. Barnett, P.M. Pinsky, Modeling electrostatic force microscopy for conductive and dielectric samples using the boundary element method, Eng. Anal. Bound. Elem. 32 (8) (2008) 682–691.
- [16] G.M. Sacha, E. Sahagún, J.J. Sáenz, A method for calculating capacitances and electrostatic forces in atomic force microscopy, J. Appl. Phys. 101 (2) (2007).
- [17] L. Fumagalli, G. Ferrari, M. Sampietro, G. Gomila, Dielectric-constant measurement of thin insulating films at low frequency by nanoscale capacitance microscopy, Appl. Phys. Lett. 91 (24) (2007).
- [18] D. El Khoury, et al., Characterization of dielectric Nanocomposites with electrostatic force microscopy, Scanning 2017 (2017) 1–14.

- [19] S. Peng, Q. Zeng, X. Yang, J. Hu, X. Qiu, J. He, Local dielectric property detection of the interface between nanoparticle and polymer in nanocomposite dielectrics, Sci. Rep. 6 (December) (2016) 1–9.
- [20] S. Lee, Using data envelopment analysis and decision trees for efficiency analysis and recommendation of B2C controls, Decis. Support. Syst. 49 (4) (2010) 486–497.
- [21] H. Chen, H. Zhao, J. Shen, R. Zhou, Q. Zhou, Supervised machine learning model for high dimensional gene data in colon cancer detection, Proc. - 2015 IEEE Int. Congr. Big Data, BigData Congr. 2015 (2015) 134–141.
- [22] A. Jain, B. Satish, Integrated approach for short term load forecasting using SVM and ANN, in: IEEE Reg. 10 Annu. Int. Conf. Proceedings/TENCON, no. March, 2008, pp. 1–6.
- [23] V. Stanev, C. Oses, I. Takeuchi, Machine learning modeling of superconducting critical temperature, NPJ Comput. Mater. 29 (May, 2018).
- [24] O.A. Castañeda-Uribe, R. Reifenberger, A. Raman, A. Avila, Depth-sensitive subsurface imaging of polymer nanocomposites using second harmonic kelvin probe force microscopy, ACS Nano 9 (3) (2015) 2938–2947.
- [25] D. El Khoury, R. Arinero, J.C. Laurentie, J. Castellon, M. Frechette, Investigation of EFM capabilities for probing interphases in nanodielectric materials: A numerical study, in: Proc. 2016 IEEE Int. Conf. Dielectr. ICD 2016 2, 2016, pp. 800–803.
- [26] D.H. Hong, C. Hwang, Support vector fuzzy regression machines, Fuzzy Sets Syst. 138 (2) (2003) 271–281.
- [27] L. Breiman, Random forests, Mach. Learn. 45 (1) (2001) 5-32.
- [28] F. Pedregosa, et al., Scikit-learn: Machine Learning in Python Gaël Varoquaux Bertrand Thirion Vincent Dubourg Alexandre Passos PEDREGOSA Pedregosa, Varoquau, Gramfort et al. Matthieu Perrot, J. Mach. Learn. Res. 12 (2011) 2825–2830.